Video Article

Exfoliation of Egyptian Blue and Han Blue, Two Alkali Earth Copper Silicate-based Pigments

Darrah Johnson-McDaniel[1], Tina T. Salguero[1]

[1]Department of Chemistry, The University of Georgia

Correspondence to: Tina T. Salguero at salguero@uga.edu

URL: http://www.jove.com/video/51686
DOI: doi:10.3791/51686

Keywords: Chemistry, Issue 86, Nanosheets, Egyptian Blue, Han Blue, Pigment, Near Infrared, Luminescence, Exfoliation, Delamination, Two-Dimensional, Ink, Colloidal Dispersion

Date Published: 4/24/2014

Citation: Johnson-McDaniel, D., Salguero, T.T. Exfoliation of Egyptian Blue and Han Blue, Two Alkali Earth Copper Silicate-based Pigments. *J. Vis. Exp.* (86), e51686, doi:10.3791/51686 (2014).

Abstract

In a visualized example of the ancient past connecting with modern times, we describe the preparation and exfoliation of $CaCuSi_4O_{10}$ and $BaCuSi_4O_{10}$, the colored components of the historic Egyptian blue and Han blue pigments. The bulk forms of these materials are synthesized by both melt flux and solid-state routes, which provide some control over the crystallite size of the product. The melt flux process is time intensive, but it produces relatively large crystals at lower reaction temperatures. In comparison, the solid-state method is quicker yet requires higher reaction temperatures and yields smaller crystallites. Upon stirring in hot water, $CaCuSi_4O_{10}$ spontaneously exfoliates into monolayer nanosheets, which are characterized by TEM and PXRD. $BaCuSi_4O_{10}$ on the other hand requires ultrasonication in organic solvents to achieve exfoliation. Near infrared imaging illustrates that both the bulk and nanosheet forms of $CaCuSi_4O_{10}$ and $BaCuSi_4O_{10}$ are strong near infrared emitters. Aqueous $CaCuSi_4O_{10}$ and $BaCuSi_4O_{10}$ nanosheet dispersions are useful because they provide a new way to handle, characterize, and process these materials in colloidal form.

Video Link

The video component of this article can be found at http://www.jove.com/video/51686/

Introduction

Vibrant colors were prized throughout the ancient world. Even today, we can still see the remains of pigments and dyes created by every major culture. Remarkably, two of the most famous synthetic blue pigments share a similar chemical composition and structure, despite having been developed at widely different times and places. The colored components of both Egyptian blue, $CaCuSi_4O_{10}$, and Han blue, $BaCuSi_4O_{10}$, belong to the alkali earth copper tetrasilicate series, $ACuSi_4O_{10}$ (A = Ca, Sr, Ba)[1], as well as the larger gillespite group, $ABSi_4O_{10}$ (B = Fe, Cu, Cr)[2,3].

Beyond traditional pigment applications, current scientific interest in these materials centers on their strong near infrared (NIR) emission properties. This emission originates from the Cu^{2+} in square planar coordination; these ions are linked by tetrahedral silicate moieties within the three-dimensional crystal structure, and the resulting layers alternate with alkali earth ions[4-6]. Recent technical highlights include NIR imaging to identify Egyptian and Han blue pigments on cultural heritage artifacts[7,8], lanthanide doping of $ACuSi_4O_{10}$ to enhance NIR reflectance properties and open new energy transfer pathways[9,10], the use of $ACuSi_4O_{10}$ as the active material for optical sensors[11], and the exfoliation of $CaCuSi_4O_{10}$ into monolayer nanosheets[12].

In particular, this last example provides a way to nanostructure $CaCuSi_4O_{10}$ so that it can be handled as a colloidal dispersion rather than as a particulate solid[12]. Because colloidal dispersions are compatible with solution-processing techniques (*e.g.* spin coating, ink jet printing, layer-by-layer deposition), this advance opens new application areas that range from security inks to biomedical imaging. The experimental protocols illustrated in this contribution will enable researchers from diverse backgrounds to prepare, characterize, and use $CaCuSi_4O_{10}$ and $BaCuSi_4O_{10}$ nanosheets in their work.

Protocol

1. Preparation of $CaCuSi_4O_{10}$

1. Melt Flux Synthesis of $CaCuSi_4O_{10}$
    1. Weigh out $CaCO_3$, SiO_2, and $Cu_2CO_3(OH)_2$ in a 2:8:1 molar ratio: 0.1331 g (1.330 mmol) of $CaCO_3$, 0.3196 g (5.319 mmol) of SiO_2, 0.1470 g (0.6648 mmol) of $Cu_2CO_3(OH)_2$. In addition, weigh out the flux components (12.5% by weight): 0.0375 g of Na_2CO_3, 0.0125 g of NaCl, and 0.0250 g of $Na_2B_4O_7{\cdot}10H_2O$. Add these materials to a clean agate mortar.
    2. Hand grind for ~5 min with an agate pestle until the mixture becomes a homogeneous light green powder (**Figures 1a** and **2a**). Transfer this mixture to a clean, dry platinum crucible.

3. Heat the crucible in a furnace to 875 °C (ramp rate of 2 °C/min), hold at 875 °C for 16 hr, and then cool down to room temperature (rate of 0.8 °C/min).
4. Remove the crystals from the crucible and gently crush them using a pestle.
5. Allow the crystals to soak in 50 ml of 1 M aqueous HCl overnight to remove the melt flux.
6. Filter the crystals and wash with deionized water to fully remove any remaining melt flux.
   Note: This material should be ground into a finer powder for powder X-ray diffraction (PXRD) analysis (**Figure 5**). It also can be characterized by optical microscopy (**Figure 3**), scanning electron microscopy (SEM) (**Figure 4**), and NIR photography (**Figure 8**).

2. Solid State Synthesis of $CaCuSi_4O_{10}$
   1. Weigh out $CaCO_3$, SiO_2, and CuO in a 1:4:1 molar ratio: 0.1331 g (1.330 mmol) of $CaCO_3$, 0.3196 g (5.319 mmol) of SiO_2, and 0.1058 g CuO (1.330 mmol) and add to a clean agate mortar.
   2. Dampen the powder mixture with 1-2 ml acetone and hand grind with an agate pestle for ~5 min. Transfer the resulting light gray powder (**Figures 1b** and **2b**) into a platinum crucible.
   3. Heat the crucible in a box furnace to 1,020 °C at a ramp rate of 5 °C/min, hold for 16 hr, and then cool down to room temperature
   4. Scrape out the loose, light blue-gray powder using a polytetrafluoroethylene (PTFE) spatula.
      Note: The product can be characterized by optical microscopy (**Figure 3**), SEM (**Figure 4**), PXRD (**Figure 5**), and NIR photography (**Figure 8**).

2. Synthesis of $BaCuSi_4O_{10}$

1. Melt Flux Synthesis of $BaCuSi_4O_{10}$
   1. Weigh out $BaCO_3$, SiO_2, and CuO in a 1:4:1 molar ratio: 0.2085 g $BaCO_3$ (1.057 mmol), 0.2539 g SiO_2 (4.226 mmol), and 0.0840 g CuO (1.056 mmol). In addition, weigh out the flux component (12.5% by weight): 0.0765 g of PbO. Add these materials to a clean agate mortar.
   2. Hand grind for ~5 min with an agate pestle until the mixture becomes a homogeneous light gray powder (**Figures 1c** and **2c**). Transfer this mixture to a clean, dry platinum crucible.
   3. Heat the crucible in a furnace to 950 °C (ramp rate of 2 °C/min), hold at 950 °C for 24 hr, then slowly cool down to 700 °C (rate of 0.1 °C/min), and finally cool to room temperature.
   4. Remove the crystals from the crucible and gently crush them using a pestle.
   5. Allow the crystals to soak in 50 ml of 1 M aqueous HNO_3 overnight to remove the melt flux.
   6. Filter the crystals and wash with deionized water to fully remove the remainder of the melt flux. Note: This material should be ground into a finer powder for PXRD analysis (**Figure 6**). It also can be characterized by optical microscopy (**Figure 3**) and NIR photography (**Figure 8**).

2. Solid State Synthesis of $BaCuSi_4O_{10}$
   1. Weigh out $BaCO_3$, SiO_2, and CuO in a 1:4:1 molar ratio: 0.2085 g $BaCO_3$ (1.057 mmol), 0.2539 g SiO_2 (4.226 mmol), and 0.0840 g CuO (1.056 mmol) and add to a clean agate mortar.
   2. Dampen the powder mixture with 1-2 ml acetone and hand grind with an agate pestle for ~5 min. Transfer the resulting light gray powder (**Figures 1d** and **2d**) into a platinum crucible.
   3. Heat the crucible in a box furnace to 960 °C at a ramp rate of 5 °C/min and hold for 16 hr, then cool to room temperature.
   4. Scrape out the loose blue powder using a polytetrafluoroethylene (PTFE) spatula. Note: The product can be characterized by optical microscopy (**Figure 3**), PXRD (**Figure 6**), and NIR photography (**Figure 8**).

3. Exfoliation of $CaCuSi_4O_{10}$

1. Charge a 50 ml round bottom flask with 0.50 g of $CaCuSi_4O_{10}$, 40 ml of deionized water, and a glass-coated magnetic stir bar.
2. Attach a water-cooled condenser to the flask. Heat the reaction to 85 °C with magnetic stirring at 400 rpm for two weeks.
3. Remove from the heat source, allow the solution to settle undisturbed overnight, and then filter the supernatant through a 0.4 µm membrane filter. Vacuum dry the solids. Note: The product is a light blue powder that can be characterized by optical microscopy (**Figure 3**), PXRD (**Figure 5**), transmission electron microscopy (TEM) (**Figure 7**), and NIR photography (**Figure 8**).

4. Exfoliation of $BaCuSi_4O_{10}$

1. Charge a 50 ml plastic centrifuge tube with 0.14 g of $BaCuSi_4O_{10}$ and 20 ml of *N*-vinyl pyrrolidone.
2. With the centrifuge tube immersed in an ice/water bath, sonicate with a probe ultrasonicator at 40% amplitude (17 W) for 1 hr.
3. Let the dispersion settle undisturbed overnight, and then decant the supernatant into a new centrifuge tube.
4. Spin down at 10,286 x g using a centrifuge. Decant the supernatant, leaving the nanosheets at the bottom of the centrifuge tube.
5. Resuspend this material in 20 ml of water with a few minutes of bath sonication. To isolate a powder, filter through a 0.4 µm membrane filter and vacuum dry the solids. Note: The product is a light blue powder that can be characterized by optical microscopy (**Figure 3**), PXRD (**Figure 6**), TEM (**Figure 7**), and NIR photography (**Figure 8**).

5. Ink Preparation

1. Disperse ~0.10 g of $CaCuSi_4O_{10}$ nanosheets in 5 ml of deionized water using bath sonication for ~10 min. Note: This ink (**Figure 9**) can be used for painting, printing, *etc.* See **Figure 10** for a representative example where the ink was applied to paper with a brush.

6. Near Infrared Photographic Imaging

1. Irradiate the samples using red light (*e.g.* with a red light-emitting diode array), taking care to eliminate any other sources of light.
2. Photograph using a camera modified to image in the near infrared region. Use f stop setting f/22 and an exposure time of 0.5 sec.

Representative Results

The described syntheses of $CaCuSi_4O_{10}$ and $BaCuSi_4O_{10}$ provide approximately 0.5 g of product per batch. Isolated yields of $CaCuSi_4O_{10}$ from the melt flux and solid-state syntheses typically range from 70-75% and 90-95%, respectively. For $BaCuSi_4O_{10}$, the isolated yields from the melt flux and solid-state syntheses typically range from 65-70% and 95-99%, respectively.

The textures of all of the prepared materials, as well as differences in the intensity of their blue color due to varying crystallite sizes, are visible by low magnification optical microscopy (**Figures 3a-h**). Scanning electron microscopy (SEM) images confirm that the solid-state method of synthesizing $CaCuSi_4O_{10}$ produces ~1-15 µm primary crystallites (**Figure 4b**) whereas melt flux conditions lead to ~5-50 µm crystallites (**Figure 4a**). Powder X-ray diffraction (PXRD) patterns for $CaCuSi_4O_{10}$ (**Figures 5a** and **5c**) and $BaCuSi_4O_{10}$ (**Figures 6a** and **6c**) showcase the composition and phase purity of these products.

Representative transmission electron microscopy (TEM) images show the nanosheet morphology of the exfoliated products (**Figure 7**). In addition, NIR photographic imaging shows the strong luminescence of both the bulk and exfoliated materials (**Figure 8**). A simple way to illustrate the solution processability of $CaCuSi_4O_{10}$ nanosheets is to prepare an aqueous ink (**Figure 9**) suitable for painting (**Figure 10**).

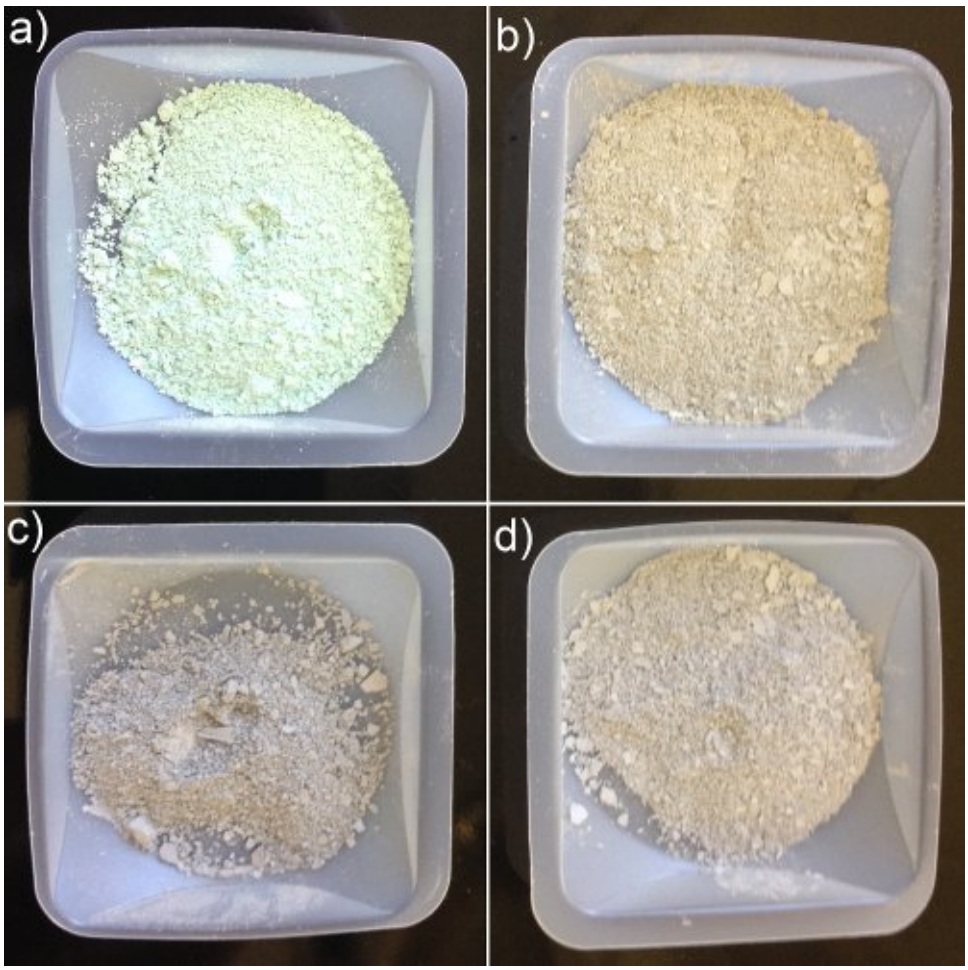

Figure 1. Photographs of the hand-ground starting materials. (**a**) $CaCuSi_4O_{10}$ melt flux, (**b**) $CaCuSi_4O_{10}$ solid-state, (**c**) $BaCuSi_4O_{10}$ melt flux, and (**d**) $BaCuSi_4O_{10}$ solid-state syntheses. Please click here to view a larger version of this figure.

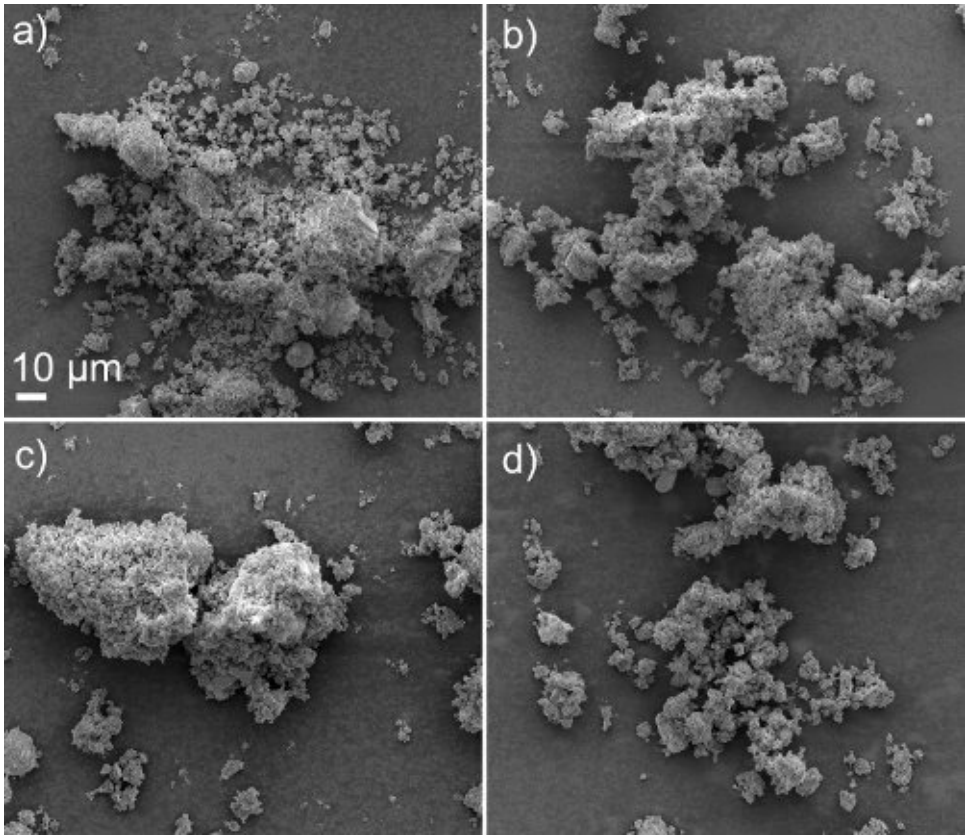

Figure 2. Scanning Electron Microscopy. Images of the hand-ground starting materials for the (**a**) $CaCuSi_4O_{10}$ melt flux, (**b**) $CaCuSi_4O_{10}$ solid-state, (**c**) $BaCuSi_4O_{10}$ melt flux, and (**d**) $BaCuSi_4O_{10}$ solid-state syntheses. All samples were coated with gold prior to imaging. Please click here to view a larger version of this figure.

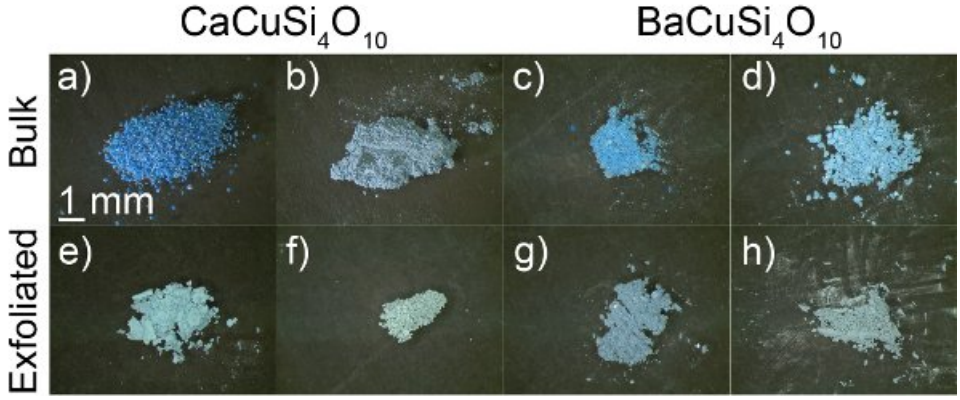

Figure 3. Optical Microscopy. Bulk $CaCuSi_4O_{10}$ prepared by melt flux (**a**) and solid state (**b**) procedures. Bulk $BaCuSi_4O_{10}$ prepared by melt flux (**c**) and solid state (**d**) procedures. Exfoliated products (**e-h**) of (**a-d**), respectively. All images share the 1 mm scale bar show in panel (**a**). Please click here to view a larger version of this figure.

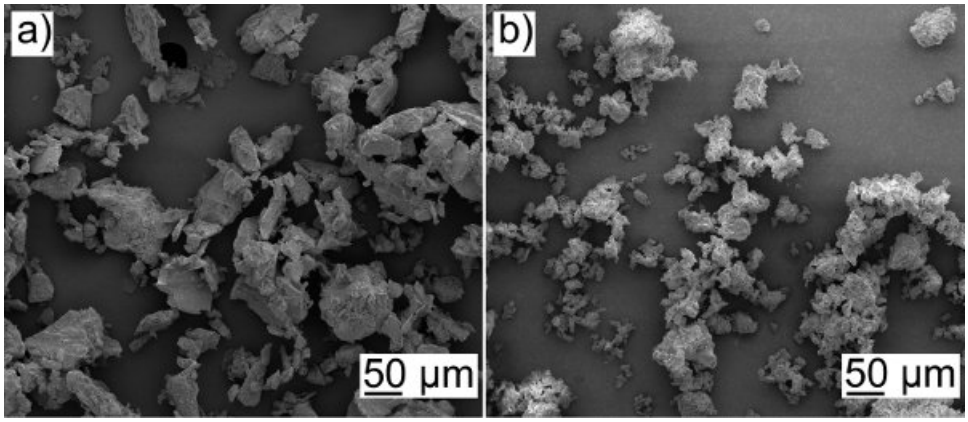

Figure 4. Scanning Electron Microscopy. Images of bulk $CaCuSi_4O_{10}$ made by melt flux (**a**) and solid state (**b**) methods. Samples were coated with gold prior to imaging. Please click here to view a larger version of this figure.

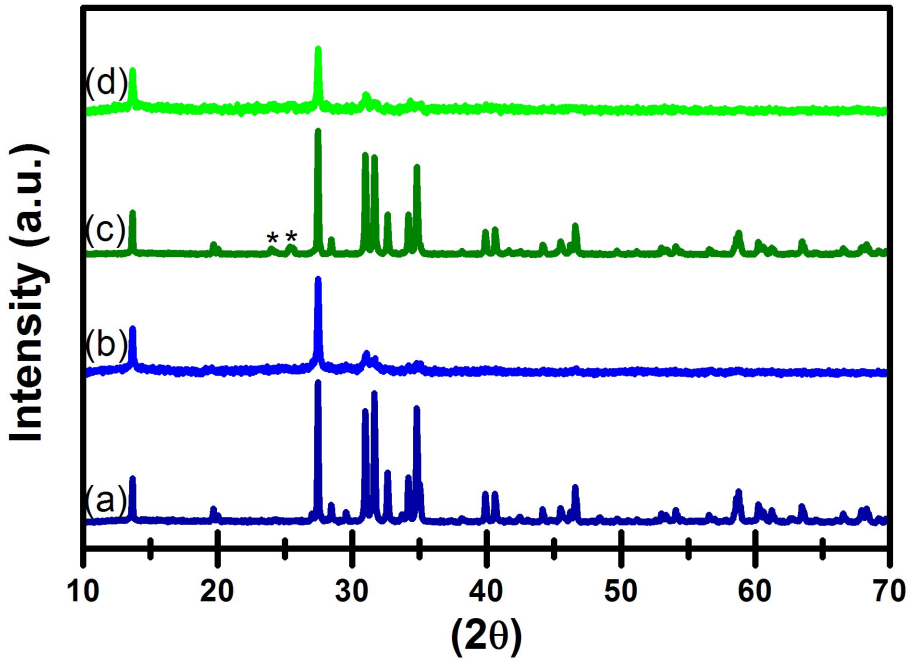

Figure 5. Powder X-Ray Diffraction: $CaCuSi_4O_{10}$. Patterns for bulk $CaCuSi_4O_{10}$ prepared by melt flux (**a**) and solid state (**c**) methods. Asterisks denote a silica impurity. Patterns for exfoliated $CaCuSi_4O_{10}$, (**b**) and (**d**), prepared from (**a**) and (**c**), respectively. Please click here to view a larger version of this figure.

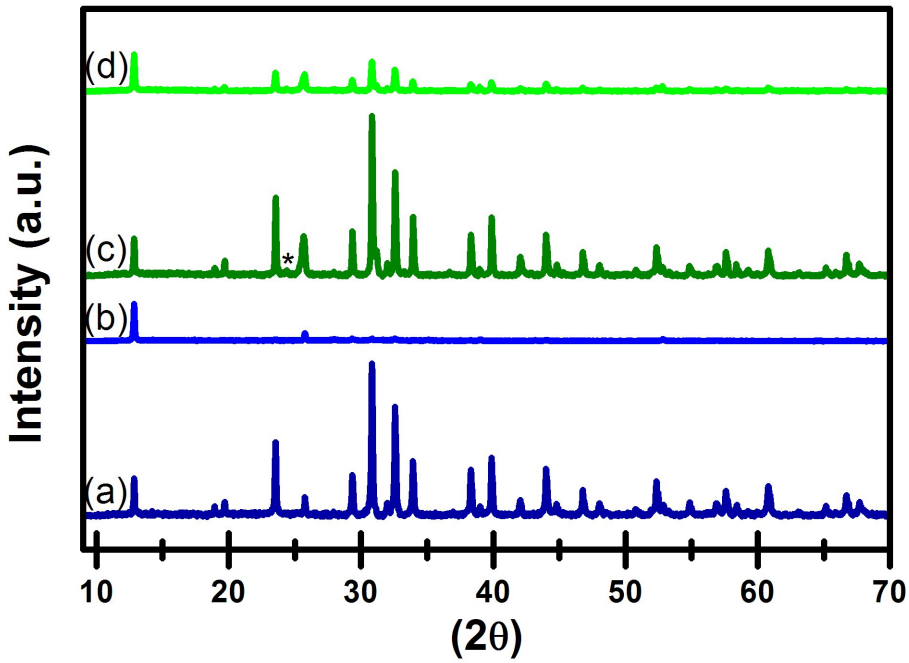

Figure 6. Powder X-Ray Diffraction: $BaCuSi_4O_{10}$. Patterns for bulk $BaCuSi_4O_{10}$ prepared by melt flux (**a**) and solid state (**c**) methods. Asterisk denotes a silica impurity. Patterns for exfoliated $BaCuSi_4O_{10}$, (**b**) and (**d**), prepared from (**a**) and (**c**), respectively. Please click here to view a larger version of this figure.

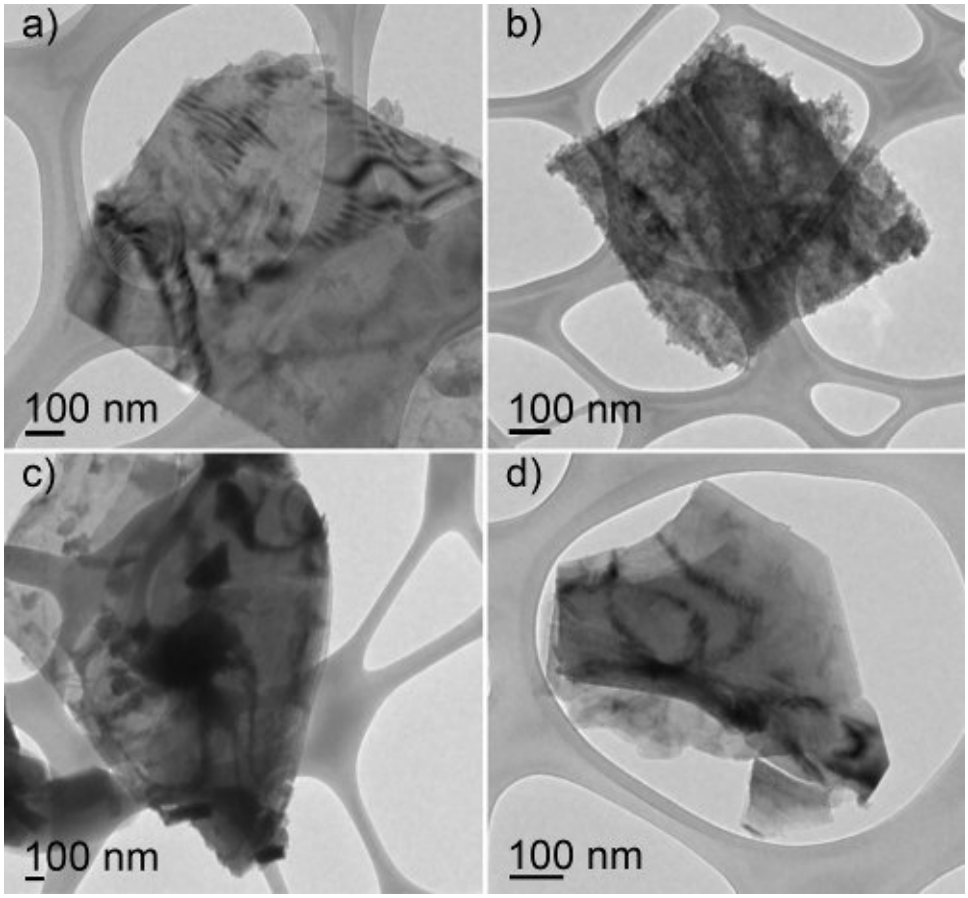

Figure 7. Transmission Electron Microscopy. Representative images of exfoliated $CaCuSi_4O_{10}$ derived from bulk $CaCuSi_4O_{10}$ made by melt flux (**a**) or solid state (**b**) methods. Representative images of exfoliated $BaCuSi_4O_{10}$ derived from bulk $BaCuSi_4O_{10}$ made by melt flux (**c**) or solid state (**d**) methods. Please click here to view a larger version of this figure.

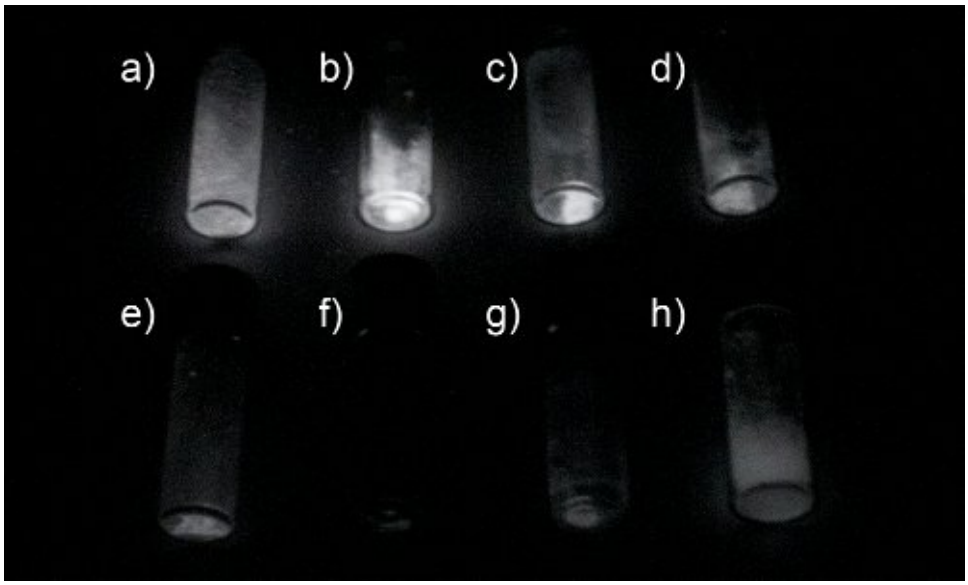

Figure 8. Near Infrared Imaging. Luminescence of bulk $CaCuSi_4O_{10}$ prepared by melt flux (**a**) and solid state (**b**) procedures. Luminescence of bulk $BaCuSi_4O_{10}$ prepared by melt flux (**c**) and solid state (**d**) procedures. Luminescence of the exfoliated products (**e-h**) of (**a-d**), respectively. Powder samples are contained within glass vials, and the entire set of samples was imaged at once. Please click here to view a larger version of this figure.

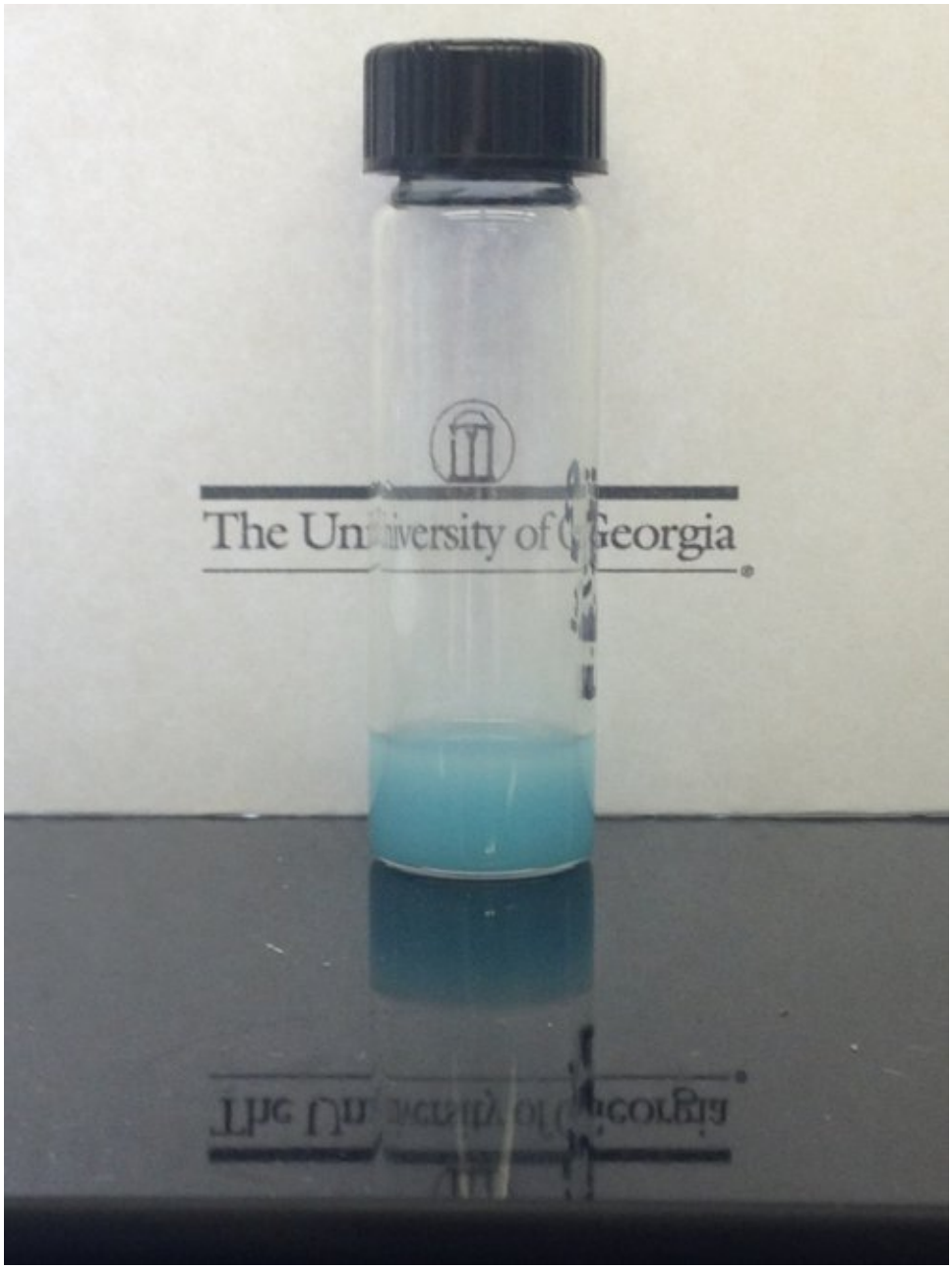

Figure 9. Photograph of a $CaCuSi_4O_{10}$ nanosheet ink in a vial.

Figure 10. Near Infrared Imaging. A rudimentary painting with the $CaCuSi_4O_{10}$ nanosheet ink that illustrates both its simple application and its luminescence properties.

Discussion

The preparation of Egyptian blue pigment, a mixture of mostly $CaCuSi_4O_{10}$ and SiO_2, is a well-studied process[4,13-21]. The numerous reported procedures may be categorized as either melt flux or solid-state reactions. Two major advantages of the melt flux approach are that it permits lower reaction temperatures (<900 °C) and allows $CaCuSi_4O_{10}$ crystals to nucleate and grow from a molten glass phase[20]. The flux component is typically an alkali salt (*e.g.* Na_2CO_3) or borate compound (*e.g.* borax). In comparison, the solid-state syntheses omit the flux but require higher temperatures (~1,000 °C) for the reaction between Ca, CuO, and SiO_2 sources to reach completion.

Although the synthesis of Han blue pigment is not as well studied as that of Egyptian blue[4,22-25], the preparation of $BaCuSi_4O_{10}$ follows similar melt flux and solid-state routes with two differences: (1) a PbO flux should be used, and (2) the reaction temperatures must be more closely controlled because of alternative Ba-Cu-Si-O phases that can form (*e.g.* $BaCuSi_2O_6$).

These points are illustrated by the detailed procedures and results described in this paper. First, for all methods, the starting materials should be ground to a smooth powder (**Figures 1a-d**) consisting of 5-20 μm particles (characterized by SEM; **Figures 2a-d**). Next, the use of a significant amount of flux (12.5% by weight) in the preparation of $CaCuSi_4O_{10}$ and $BaCuSi_4O_{10}$ leads to highly crystalline products, which are characterized by intense blue coloration (**Figures 3a** and **3c**), relatively large particle sizes (**Figure 4a**), and strong PXRD patterns (**Figures 5a** and **6a**). The diminished isolated yields (~70%) from these preparations are caused by adhesion of the melted reaction mixtures to the crucible. In comparison, $CaCuSi_4O_{10}$ and $BaCuSi_4O_{10}$ prepared by the solid-state route exhibit less intense coloration (**Figures 3b** and **3d**) and smaller particle sizes (**Figure 4b**). As synthesized, these products are powders that can be isolated in near-quantitative yields. Thus, for both $CaCuSi_4O_{10}$ and $BaCuSi_4O_{10}$, the advantages of flux and the importance of reaction temperature cannot be overstated.

Remarkably, the exfoliation of $CaCuSi_4O_{10}$ and $BaCuSi_4O_{10}$ occurs under simple aqueous conditions. In the case of $CaCuSi_4O_{10}$, this reaction is quite slow at room temperature (≥6 weeks to see any appreciable exfoliation), but it becomes synthetically useful at 80 °C (substantial exfoliation after 2 weeks). In comparison, the exfoliation of $BaCuSi_4O_{10}$ is sluggish even at 80 °C, and so we apply an even greater energy input in the form of ultrasonication. These reactions are highly reliable with two caveats. For $CaCuSi_4O_{10}$, it is important to use a glass-coated stir bar; if a standard PTFE-coated stir bar is used, we find that PTFE byproducts contaminate the $CaCuSi_4O_{10}$ nanosheet product. For $BaCuSi_4O_{10}$, it is important to control the ultrasonication power and time so that the reaction is stopped before the nanosheets become degraded.

Transmission electron microscopy (TEM) of the nanosheet products shows that these very thin materials have lateral dimensions ranging from hundreds of nanometers to several microns. In general these lateral dimensions correlate with the crystallite size of the three-dimensional starting material. In prior work, atomic force microscopy provided topographic mapping that demonstrated the single-layer thicknesses (~1.2 nm) of these nanosheets[12]. Photographs of powder $CaCuSi_4O_{10}$ and $BaCuSi_4O_{10}$ nanosheet samples (**Figures 3e-h**) show that their color is less intense than that of the starting materials, a direct result of nanostructuring.

Additional information is provided by PXRD (**Figures 5** and **6**), which reveals basal cleavage along the (001) plane and preferred orientation along the {00*l*} series for all nanosheet samples. These features reflect the stacked alignment of these highly anisotropic nanomaterials when drop-cast onto a substrate. Furthermore, the characteristic NIR emission of $CaCuSi_4O_{10}$ at ~910 nm and $BaCuSi_4O_{10}$ at ~950 nm is illustrated in a NIR photograph of all eight samples (**Figure 8**).

The solution processing of $CaCuSi_4O_{10}$ can be accomplished by simply preparing a colloidal dispersion of $CaCuSi_4O_{10}$ nanosheets (**Figure 9**) to use as an ink. This ink then can be applied to a substrate via spin coating, spray coating, ink jet printing[12], or simply brushing (**Figure 10**). Importantly, the NIR emission properties of $CaCuSi_4O_{10}$ are retained at all stages of this process. These new possibilities highlight the contrast between $CaCuSi_4O_{10}$ nanosheets and the traditional use of Egyptian blue pigment, a highly granular material that is challenging to incorporate into a smooth paint.

Disclosures

The authors have no competing financial interests.

Acknowledgements

We thank Prof. Mark Abbe (UGA) for providing the NIR imaging equipment and Dr. Rasik Raythatha (Solvay Performance Chemicals) for the barium carbonate used in this work. We acknowledge the efforts of Isaiah Norris (UGA undergraduate) and Terra Blevins (North Oconee High School), who helped test the synthetic methods.

References

1. Berke, H. The Invention of Blue and Purple Pigments in Ancient Times. *Chem. Soc. Rev.* **36**, 15-30, doi: 10.1039/B606268G (2007).
2. Hazen, R. M., Burnham, C. W. The Crystal Structure of Gillespite I and II: A Structure Determination at High Pressure. *Am. Min.* **59**, 1166-1176 (1974).
3. Miletich, R., Allan, D. R., Angel, R. J. The Synthetic Cr^{2+} Silicates $BaCrSi_4O_{10}$ and $SrCrSi_4O_{10}$: The Missing Links in the Gillespite-Type $ABSi_4O_{10}$ Series. *Am. Min.* **82**, 697-707 (1997).
4. Pabst, A. Structures of Some Tetragonal Sheet Silicates. *Acta Cryst.* **12**, 733-739, doi: 10.1107/S0365110X5900216X (1959).
5. Chakoumakos, B. C., Fernandez-Baca, J. A., Boatner, L. A. Refinement of the Structures of the Layer Silicates $MCuSi_4O_{10}$ (M = Ca, Sr, Ba) by Rietveld Analysis of Neutron Powder Diffraction Data. *J. Solid State Chem.* **103**, 105-113, doi: 10.1006/jssc.1993.1083 (1993).
6. Hughes, E. M., Pack, M. J., Dann, S. E., Weller, M. T. Preparation and Structural Characterisation of Alkaline Earth Sheet Silicates Containing Copper by Powder Neutron Diffraction, EXAFS and UV-Visible Spectroscopy. *Anales de Quimica Int. Ed.* **93**, 233-236 (1997).
7. Accorsi, G. *et al.* The Exceptional Near-Infrared Luminescence Properties of Cuprorivaite (Egyptian Blue). *Chem. Comm.* 3392-3394, doi: 10.1039/B902563D (2009).
8. Verri, G. The Spatially Resolved Characterization of Egyptian Blue, Han Blue and Han Purple by Photo-Induced Luminescence Digital Imaging. *Anal. Bioanal. Chem.* **394**, 1011-1021, doi: 10.1007/s00216-009-2693-0 (2009).
9. Jose, S., Reddy, M. L. Lanthanum-Strontium Copper Silicates as Intense Blue Inorganic Pigments with High Near-Infrared Reflectance. *Dyes Pigm.* **98**, 540-546, doi: 10.1016/j.dyepig.2013.04.013 (2013).
10. Zhuang, Y., Tanabe, S. Forward and Back Energy Transfer Between Cu^{2+} and Yb^{3+} in $Ca_{1-x}CuSi_4O_{10}$:Yb_x Crystals. *J. Appl. Phys.* **112**, 093521, doi: 10.1063/1.4765013 (2012).
11. Borisov, S. M., Würth, C., Resch-Genger, U., Klimant, I. New Life of Ancient Pigments: Application in High-Performance Optical Sensing Materials. *Anal. Chem.* **85**, 9371-9377, dx.doi.org/10.1021/ac402275g (2013).
12. Johnson-McDaniel, D., Barrett, C. A., Sharafi, A., Salguero, T. T. Nanoscience of an Ancient Pigment. *J. Am. Chem. Soc.* **135**, 1677-1679, doi:10.1021/ja310587c (2013).
13. Laurie, A. P., McLintock, W. F. P., Miles, F. D. Egyptian Blue. *Proc. R. Soc. London A.* **89**, 418-429, doi: 10.1098/rspa.1914.0010 (1914).
14. Chase, W. T. Egyptian Blue as a Pigment and Ceramic Material. In *Science in Archaeology*, Brill, R. H., Ed. MIT Press: Cambridge, MA 80-90 (1971).
15. Tite, M. S., Bimson, M., Cowell, M. R. Chapter 11: Technological Examination of Egyptian Blue. In *Archaeological Chemistry III, Advances in Chemistry Series*. (vol. 205), Lambert, J. B., Ed. pp. 215-42, American Chemical Society: Washington, DC (1984).
16. Ullrich, D. Egyptian Blue and Green Frit: Characterization, History and Occurrence, Synthesis. In *Datation-Charactérisation des Peintures Pariétales et Murales*. F. Delamare, F., Hackens, T., Helly, B. Eds. PACT 17, È. Ollefe, Rixensart, Belgium 323-332 (1987).
17. Riederer, J. Chapter 1: Egyptian Blue. In *Artist' Pigments: A Handbook of Their History and Characteristics*. Vol. 3, Fitzhugh, E. W. Ed., National Gallery of Art: Washington, DC 23-45 (1997).
18. Delamare, F. Sur les Processus Physiques Intervenant Lors de la Synthèse du Bleu Égyptien: Réflexion à Propos de la Composition de Pigments Bleus Gallo-Romains. *Revue d'Archéométrie.* **21**, 103-119 (1997).
19. Canti, M.G., Heathcote, J.L., Microscopic Egyptian Blue (Synthetic Cuprorivaite) from Sediments at Two Archaeological Sites in West Central England. *J. Arch. Sci.* **29**, 831-836, doi: 10.1006/jasc.2001.0717 (2002).
20. Pradell, T., Salvado, N., Hatton, G.D., Tite, M.S., Physical Processes Involved in Production of the Ancient Pigment, Egyptian Blue. *J. Am. Ceram. Soc.* **89**, 1426-1431, doi: 10.1111/j.1551-2916.2005.00904.x (2006).
21. Warner, T. E. *Synthesis, Properties and Mineralogy of Important Inorganic Materials.* Wiley: Hoboken, NJ 26-47 (2011).
22. Lin, H. C., Liao, F. L., Wang, S. L. Structure of $BaCuSi_4O_{10}$. *Acta Cryst.* **C48**, 1297-1299, doi: 10.1107/S0108270192001203 (1992).
23. Janczak, J.; Kubiak, R. Refinement of the Structure of Barium Copper Silicate $BaCu[Si_4O_{10}]$ at 300 K. *Acta Cryst.* **C48**, 1299-1301,doi: 10.1107/S0108270191014580 (1992).
24. Wiedemann, H. G., Bayer, G. Formation and Stability of Chinese Barium Copper-Silicate Pigments. In *Conservation of Ancient Sites on the Silk Road: Proceedings of an International Conference on the Conservation of Grotto Sites*. Agnew, N., Ed., pp. 379-387, Getty Conservation Institute: Los Angeles (1997).
25. Berke, H., Wiedemann, H. G. The Chemistry and Fabrication of the Anthropogenic Pigments Chinese Blue and Purple in Ancient China. *East Asian Science, Technology, and Medicine*. **17**, 94-120 (2000).